Two more, bright, $z > 6$ quasars from VST ATLAS and WISE

B. Chehade,[1]★ A. C. Carnall,[1,2]† T. Shanks,[1]‡ C. Diener,[3] M. Fumagalli,[1,4] J.R. Findlay,[5] N. Metcalfe,[1] J. Hennawi,[6] C. Leibler,[7] D.N.A. Murphy,[3] J.X. Prochaska,[7] M.J. Irwin[3] & E. Gonzalez-Solares[3]

[1]Centre for Extragalactic Astronomy, Department of Physics, Durham University, South Road, Durham DH1 3LE, UK
[2]Institute for Astronomy, University of Edinburgh, Royal Observatory Edinburgh, UK
3 Institute of Astronomy, Madingley Road, Cambridge CB3 0HA, UK
[4]Institute for Computational Cosmology, Department of Physics, Durham University, South Road, Durham DH1 3LE, UK
[5]Department of Physics and Astronomy, University of Wyoming, 1000 E. University, Department 3905, Laramie, WY 82071, USA
[6]Max-Planck-Institut fur Astronomie, Konigstuhl 17, D-69117 Heidelberg, Germany
[7]University of California Observatories-Lick Observatory, University of California, 1156 High Street, Santa Cruz, CA 95064, USA; USA

Accepted 2018 February 23. Received 2018 February 22; in original form 2017 June 1.

ABSTRACT

Recently, Carnall et al. discovered two bright high redshift quasars using the combination of the VST ATLAS and WISE surveys. The technique involved using the 3-D colour plane $i-z : z-W1 : W1-W2$ with the WISE $W1$(3.4 micron) and $W2$ (4.5 micron) bands taking the place of the usual NIR J band to help decrease stellar dwarf contamination. Here we report on our continued search for $5.7 < z < 6.4$ quasars over an $\approx 2\times$ larger area of ≈ 3577 deg^2 of the Southern Hemisphere. We have found two further $z > 6$ quasars, VST-ATLAS J158.6938-14.4211 at $z = 6.07$ and J332.8017-32.1036 at $z = 6.32$ with magnitudes of $z_{AB} = 19.4$ and 19.7 mag respectively. J158.6938-14.4211 was confirmed by Keck LRIS observations and J332.8017-32.1036 was confirmed by ESO NTT EFOSC-2 observations. Here we present VLT X-shooter Visible and NIR spectra for the four ATLAS quasars. We have further independently rediscovered two $z > 5.7$ quasars previously found by the VIKING/KiDS and PanSTARRS surveys. This means that in ATLAS we have now discovered a total of six quasars in our target $5.7 < z < 6.4$ redshift range. Making approximate corrections for incompleteness, we find that our quasar space density agrees with the SDSS results of Jiang et al. at $M_{1450\text{Å}} \approx -27$. Preliminary virial mass estimates based on the CIV and MgII emission lines give black hole masses in the range $M_{BH} \approx 1 - 6 \times 10^9 M_\odot$ for the four ATLAS quasars.

Key words: quasars: general - quasars: individual: VST-ATLAS J158.6938-14.4211 - quasars: individual: VST-ATLAS J332.8017-32.1036

1 INTRODUCTION

High redshift quasars are key probes of the Universe within the first billion years to redshift $z \sim 6$. Firstly, they provide observational constraints on the evolution of the quasar luminosity and black hole mass functions to the highest redshifts (Willott et al. 2005, 2010a, 2010b, Jiang et al. 2009, 2016). The existence of a high spatial density of luminous quasars at $z > 6$ would be a challenge to the standard cosmological model, which is limited in its capacity to produce large black hole masses, assuming Gaussian initial conditions (e.g. Rosas-Guevara et al. 2016).

Secondly, analysis of damped Lyα systems (DLAs) and Lyman Limit Systems (LLS) along quasar lines of sight at intermediate redshifts ($z \approx 3$) provide invaluable constraints on galaxy evolution by probing conditions within the interstellar medium (ISM) and circumgalactic medium (CGM) (e.g. Fumagalli et al. (2016), Wotta et al. (2016), Lehner et al. (2016) and

★ E-mail: benchehade@gmail.com
† E-mail: adamc@roe.ac.uk
‡ E-mail: tom.shanks@durham.ac.uk

Quasar	i (AB)	z (AB)	Y	J	H	K	$W1$	$W2$
VST-ATLAS J332.8017-32.1036	>21.84	19.75 ± 0.06	19.43 ± 0.06	18.98 ± 0.05	18.43 ± 0.07	17.85 ± 0.07	16.36 ± 0.05	15.57 ± 0.09
VST-ATLAS J158.6938-14.4211	>21.56	19.44 ± 0.08	18.78 ± 0.07	18.27 ± 0.06	17.58 ± 0.09	16.86 ± 0.08	15.86 ± 0.08	15.13 ± 0.13
PSO J340.2041-18.6621	>22.5	19.44 ± 0.10	-	-	-	17.69 ± 0.19	16.56 ± 0.07	15.53 ± 0.13

Table 1. VST-ATLAS (i,z), VHS (Y,J,H,K) and ALLWISE (W1,W2) magnitudes for three quasars newly selected from the VST ATLAS survey. None of the quasars were detected in the i band and 3σ limiting magnitudes are provided. PSO J340.2041-18.6621 was previously discovered by Bañados et al. (2014). All magnitudes are on the Vega system except where indicated.

references therein), via absorber metallicities, covering factors and kinematics. Some progress has been made in extending these analyses to higher redshifts (e.g. Rafelski et al. (2014),Crighton et al. (2015), Wang et al. (2015)).

Finally, high redshift quasars cast light on conditions in the intergalactic medium (IGM) during the epoch of reionisation. Studies have been made of the Lyα emission-line profiles of these objects, their ionized near zones and the Gunn-Peterson troughs in their spectra (e.g. Becker et al. (2001), Fan et al. (2006), Carilli et al. (2010), Venemans et al. (2015b) and Barnett et al. (2017)) producing a general consensus view of a patchy reionisation which ended around $z = 5 - 6$.

There has also been much debate about the relative contributions of active galactic nucleus (AGN) activity and star formation to the reionization of the IGM, and the luminosity function of high redshift quasars is a crucial variable in this context. Whilst it has been shown (McLeod et al. 2015, 2016) that star formation in high redshift galaxies can provide the bulk of the ionizing photons necessary for reionization, the actual fractional contributions from AGN and star formation are still unknown, with Madau & Haardt (2015) presenting a plausuble scenario in which AGN activity provides the majority of the ionizing photons. The major extra AGN contribution in their work is due to the increased slope of the faint end of the quasar luminosity function found in the CANDELS survey by Giallongo et al. (2015). However, using the same CANDELS data, Parsa et al. (2018) report no evidence for a significant AGN contribution. Although here we shall be addressing the bright end only, the importance of determining the quasar luminosity function at high redshift is clear not only for the source of reionising photons but also for models of black hole seeding, growth, feedback and evolution. Clearly, bright, high redshift, quasars are also easier to follow-up for the above ISM, CGM and IGM absorption studies.

The techniques employed to detect high redshift quasars are based on essentially the same Lyman-dropout technique as has been applied for many years, where objects with a very red colour, often implied by a non-detection in a bluer band, are selected from large area sky surveys. One of the first applications of this technique was by Shanks et al. (1983) who looked for U and B dropouts relative to their R band magnitudes to find a quasar at $z = 3.63$. This method has evolved more recently to redder dropout bands in order to probe higher redshifts. However, due to the decreasing spatial density of quasars at increasingly high redshifts, contaminant objects such as cool L and T dwarf stars become more and more problematic. Due to this, a variety of new methods have recently been developed for cleaning photometrically selected samples before spectroscopic follow-up observations are made to confirm the nature of the sources.

The first study to be sensitive to quasars above $z = 6$ was reported by Fan et al. (2001, 2006) and Jiang et al. (2016) using data from the Sloan Digital Sky Survey (SDSS). They looked for i band dropouts relative to their z band magnitudes and then obtained follow-up J band imaging, selecting quasars as objects with blue $z - J$ colour to exclude cool dwarf stars. The same approach has also been applied to other survey data e.g. by Willott et al. (2010a), Venemans et al. (2015a) and Wang et al. (2017). More recently, large area Y band surveys have been used instead of follow-up J band photometry by Bañados et al. (2014, 2016) and Reed et al. (2015). A Bayesian statistical approach to candidate selection has also been developed by Mortlock et al. (2012) and Matsuoka et al. (2016). Most recently the dropout method has been applied to the z band by Venemans et al. (2013, 2015b) to begin selecting quasars at $z \gtrsim 6.5$, with the current record holder being a quasar at $z = 7.54$ discovered by Bañados et al. (2018).

In this paper we follow Carnall et al. (2015) (hereafter C15) who found two $z > 6$ quasars using the combination of the new Very Large Telescope Survey Telescope ATLAS (VST ATLAS, Shanks et al. 2015) and Wide-field Infrared Survey Explorer (WISE, Wright et al. 2010) surveys, by applying a similar method to a greater area of VST ATLAS imaging which yielded the discovery of two more bright $z > 6$ quasars.

In Section 2 we review the survey data, and in Section 3 we review our quasar selection technique. In Section 4 we report on follow-up spectroscopic observations of two further high redshift quasar candidates, which we confirm to be two new quasars at $z = 6.32$ and $z = 6.07$. In Section 5 we make an approximate estimate of the bright end of the quasar luminosity function from our new quasars plus the others found within our search area. We present our conclusions in Section 7.

All VST ATLAS magnitudes are given on the AB system, all other magnitudes are on the Vega system. All cosmological calculations assume the density parameters $\Omega_m = 0.3$, $\Omega_\Lambda = 0.7$ and Hubble Constant $h = 0.7$, with h measured in units of $100\mathrm{kms}^{-1}\mathrm{Mpc}^{-1}$.

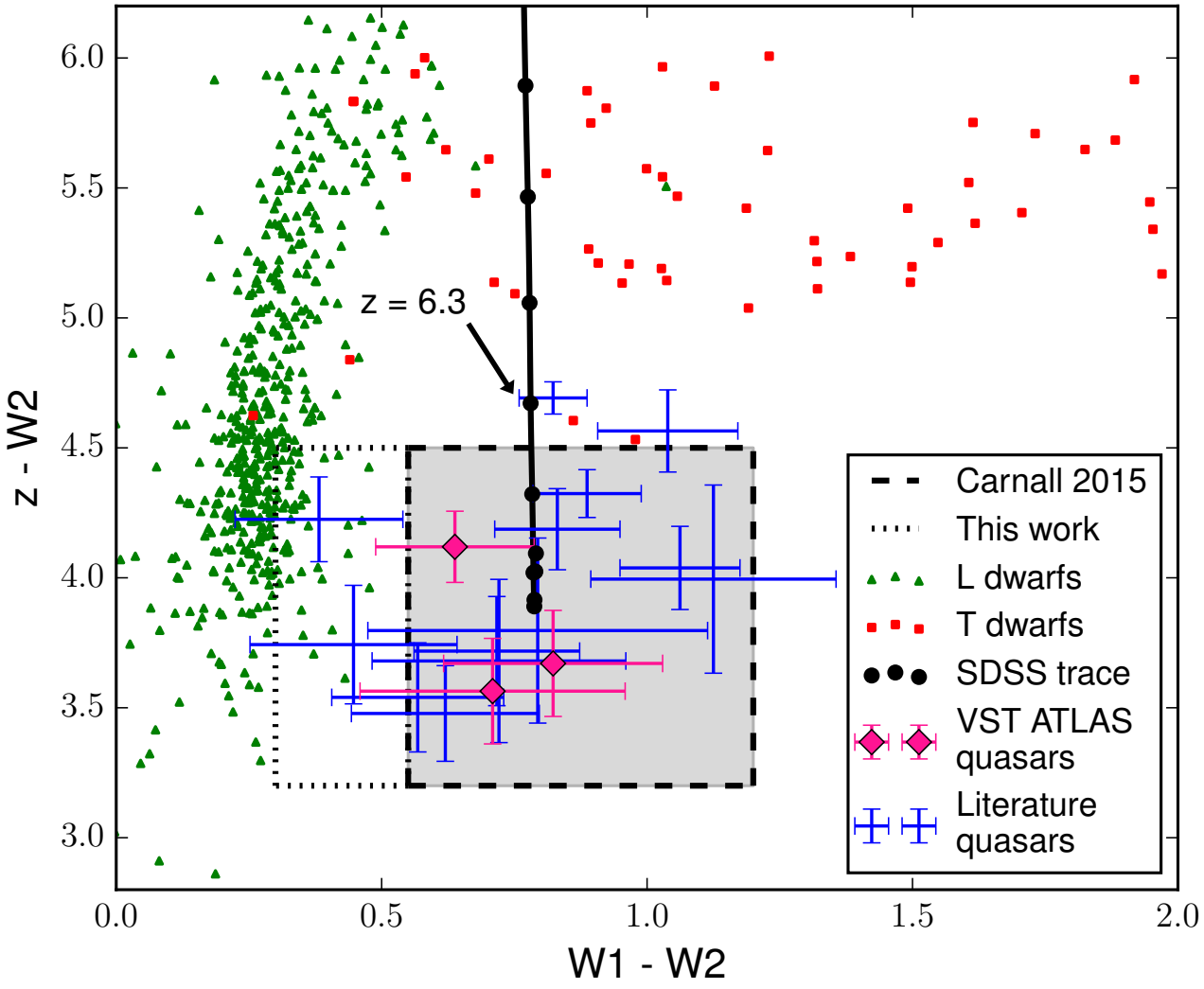

Figure 1. The $z - w2 : W1 - W2$ colour plane with the positions of 4 ATLAS quasars marked. Also marked are the positions of L and T dwarf stars and other quasars from the literature. The dashed-line box shows the colour selection of C15. The dotted line extends this selection bluewards in $W1 - W2$ to $W1 - W2 > 0.3$, including two previously discovered quasars from SDSS and with the aim of testing the completeness of the C15 selection. The black line is predicted quasar redshift track marked in 0.1 redshift intervals from $z = 5.8$ to $z = 6.6$.

2 SURVEY DATA

2.1 VST ATLAS

The VLT Survey Telescope (VST) is a 2.6 m wide-field survey telescope with a $1^\circ \times 1^\circ$ field of view. The OmegaCAM camera (Kuijken et al. 2004) consists of 32 CCDs with $2k \times 4k$ pixels, resulting in $16k \times 16k$ image with a pixel scale of $0.''21$. The VST ATLAS is a nearly completed photometric survey that will cover ≈ 4700 deg^2 of the southern extragalactic sky with coverage in *ugriz* bands. The survey takes two sub-exposures of 2×60s (u), 2×50s (g), 2×45s (r), 2×45s (i), 2×45s (z), per 1 degree field with a small dither in X and Y to cover most interchip gaps. The sub-exposures are then reduced and stacked by the Cambridge Astronomy Survey Unit (CASU). Their pipeline outputs catalogues cut at $\approx 5\sigma$ and provide fixed aperture fluxes and morphological classifications of detected objects (see Shanks et al. (2015) for more details). Here, for stellar photometry, we use a $1''$ radius aperture (i.e. `aper3`). ATLAS photometry is calibrated using the APASS Nightly zero-points (`NIGHTZPT` in the FITS headers, see Shanks et al. 2015). The star-galaxy classification is that supplied as default in the CASU catalogues and discussed in detail (by González-Solares et al. 2008).

VST ATLAS provides *ugriz* photometry to similar depths as SDSS for galaxies and up to 0.7 mag fainter (e.g. in the z-band) for stars, mainly due to its $\approx 40\%$ better seeing (e.g. $0.''81$ versus $1.''18$ in i, Shanks et al. 2015). In terms of

Quasar	Redshift	Observation Date	ESO Project No.	DIMM Seeing
VST-ATLAS J025.6821-33.4627	6.31 ± 0.03	19/11/15	096.A-0418(A)	1.″2
VST-ATLAS J029.9915-36.5658	6.02 ± 0.03	22/02/15	294.A-5031(B)	1.″2
VST-ATLAS J332.8017-32.1036	6.32 ± 0.03	24/10/15	096.A-0418(A)	1.″5
VST-ATLAS J158.6938-14.4211	6.07 ± 0.03	23/01/16	096.A-0418(B)	1.″4

Table 2. Details for VLT X-shooter observations. DIMM refers to Differential Image Motion Monitor atmospheric seeing estimates from ESO. Redshifts were estimated from the wavelengths of the Lyα emission line the X-shooter spectra. For J158-14 and J332-32 these differed slightly from the discovery spectrum redshifts reported in Sections 4.1.1 and 4.2.1.

VST−ATLAS progress at the time of this study,the survey area had increased to 3577 deg^2 from the 2060 deg^2 available to C15, partly by only using *riz* band-merged CASU catalogues. This maximises the searchable area because the *u* and *g* sky coverage is less than for *riz*. Further, the CASU database has higher sky coverage than the public accessible Edinburgh Wide Field Astronomy Unit (WFAU) archive. The average 5σ limits of the ATLAS *riz* catalogue for point sources as measured in a 1″ radius aperture are $r < 22.7$, $i < 22.0$ and $z < 20.9$ mag. See Shanks (2016) for a comparison of ATLAS parameters with various other surveys.

The main issues with the CASU catalogues are that they are currently CCD based rather than tile based (as at the WFAU). This leads to increased incompleteness in the matching at the edges which increases the numbers of spurious *r*- and *i*-band dropouts.

2.2 WISE

The Wide-field Infrared Survey Explorer (WISE, Wright et al. 2010) survey covers the mid-IR 3.4 (W1), 4.6 (W2), 12 (W3) and 22 (W4) micron bands. The advantage of WISE is its 100% coverage of ATLAS at the present time and the excellent matching of both the W1 and W2 bands' depths to VST ATLAS. The approximate 5σ limits for AllWISE[1] point sources are $W1 = 16.90$ and $W2 = 15.95$ mag in the Vega system. The W1 and W2 bands have point spread functions (PSFs) of 6.″1 and 6.″4 respectively, compared with ≈ 0.″85 in the VST ATLAS *riz* bands. Astrometric tests[2] between WISE and USNO CCD Astrograph Catalog (UCAC3) positions shows < 0.″5 rms offset between the two catalogues to the W1 limit. ATLAS optical photometry was matched to the publicly available ALLWISE Catalogue using a 3″ matching radius. For the sky density of WISE sources at $|b| > 30°$ we calculate that ≈ 4% of candidates identified in WISE will have a blended WISE source within 3″. In looking for rare, high-*z*, quasars, WISE blends (and other artefacts) will therefore have to be eliminated by visual inspection.

3 PHOTOMETRIC QUASAR SELECTION

C15 used ATLAS $i - z$ colour to select dropout candidates, then the $z - W2 : W1 - W2$ colour plane to discriminate between dwarf stars and high redshift quasars, as shown in Figure 1. $W1 - W2$ colour is the main discriminator against L dwarfs and $z - W2$ is used to discriminate between T dwarfs and quasars, providing good separation out to $z = 6.3$ before the quasar colour track crosses the T dwarf locus. Application of this technique to the first 2060 deg^2 of VST ATLAS imaging resulted in the discovery of two $z > 6$ quasars, ATLAS J029.9915-36.5658 at $z = 6.02 \pm 0.03$ and ATLAS J025.6821-33.4627 at $z = 6.31 \pm 0.03$ and the re-discovery of VIKING/KiDS J0328-3253 at $z = 5.86 \pm 0.03$.

Following C15 we first produced a list of high redshift ($z > 5.7$) quasar candidates by applying the following selection criteria to the CASU band-merged catalogues:

(i) Objects must have $18 < z_{AB} < 20$ mag, measured in a 1″ aperture (labelled as `aper3` in the CASU and WFAU catalogues). Chehade (2016) shows that this aperture provides the best balance between *S*/*N* and accuracy of the aperture corrections for point sources. The $z_{AB} > 18$ cut reduces the number of candidates for visual inspection in a range where the star /quasar number ratio is expected to increase.
(ii) Objects must be identified as a point source by their curve of growth (see González-Solares et al. 2008). Morphology is stored under the flag `Classification` where −1 is for point sources and +1 is for extended sources. We disregard morphological classification in the *i*-band, since at low *S*/*N*, the `Classification` is unreliable. Chehade et al. (2016) tests the CASU morphological classification and finds it to be ≈ 90% complete for the *g* and *r* bands. We examine the *z*-band specifically in Section 5.2.

[1] http://wise2.ipac.caltech.edu/docs/release/allwise/
[2] http://wise2.ipac.caltech.edu/docs/release/allsky/expsup/sec2_2.html

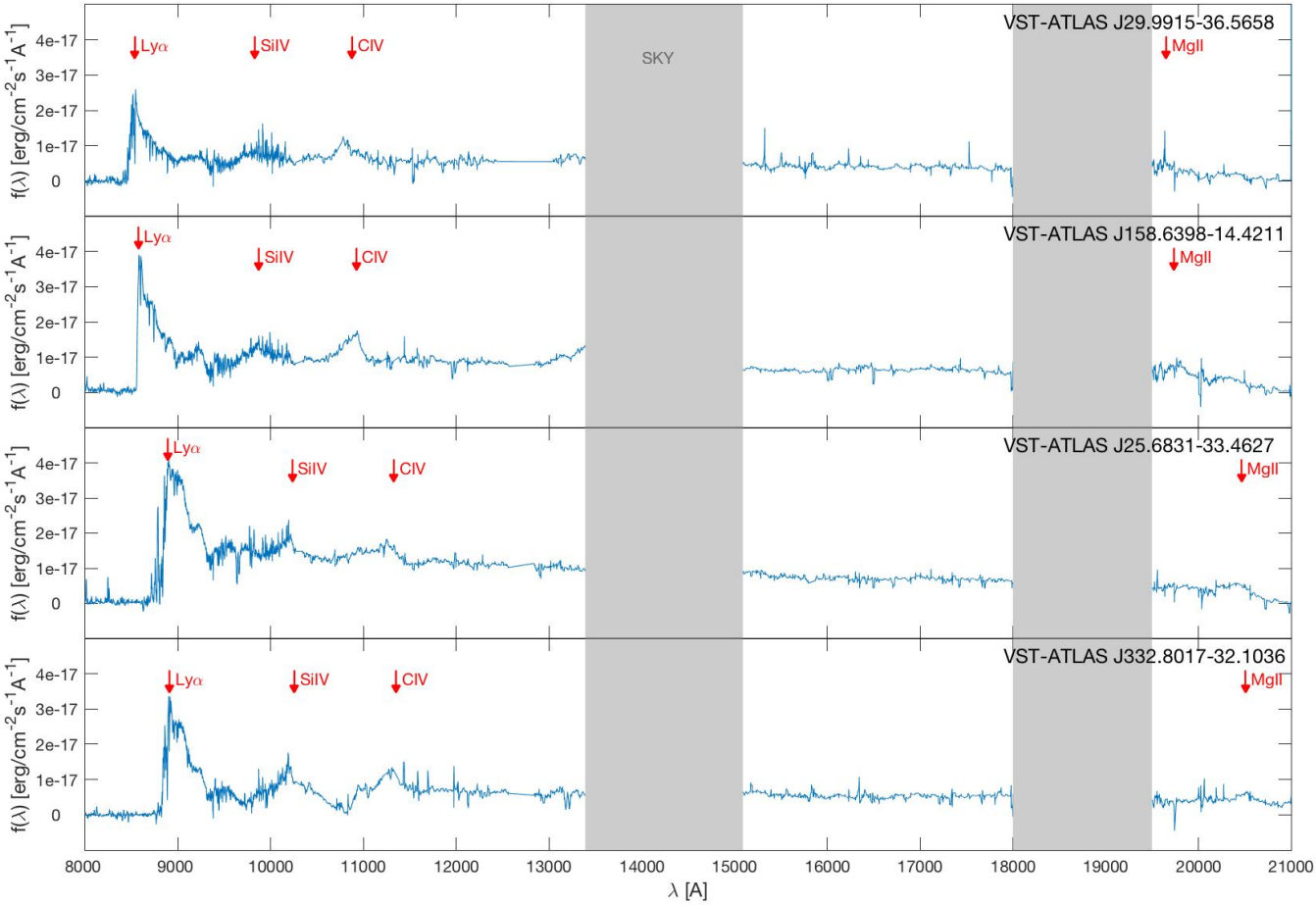

Figure 2. The VLT X-shooter spectra for our 4 ATLAS quasars. (See Table 2 for observational details). The spectra were flux calibrated to the observed z-band magnitudes from VST ATLAS and corrected for telluric absorption as described in Section 4.3. The positions of the Lyα, Si IV, C IV and MgII emission lines are marked at the redshifts given in Table 2. We note that higher ionisation lines such as C IV are frequently found to be blueshifted with respect to lower ionisation lines like Lyα and this is seen to be the case for all four quasars.

(iii) Objects must either be undetected in the i-band, or if detected must have $i - z > 2.2$. An additional selection was also carried out for which this limit was relaxed to $i - z > 1.8$, to fill observing gaps between higher priority targets. Objects must also be undetected in the u, g and r bands.
(iv) Objects must have a corresponding source in the ALLWISE catalogue within a $3''$ radius with $\frac{S}{N} > 3$ in both the W1 ($\lesssim 17.9$ mag) and W2 ($\lesssim 17.0$ mag) bands.
(v) Objects must have colours in the range $0.55 < W1 - W2 < 1.2$ and $3.2 < z_{AB} - W2 < 4.5$ (see Figure 1).

This left ≈ 130 candidates for visual inspection. The candidates were largely obviously misidentified as dropouts due to defects in the band-merging process, or in areas where the i−band seeing was poor ($> 1.''2$), meaning the dropout status could not be confirmed due to a lower limiting colour. We also limited our selection regions to the doubly exposed regions of the VST ATLAS stack (see Shanks et al. 2015) for this reason. This reduced the searchable area per tile from ~ 1 deg^2 to ~ 0.8 deg^2.

As well as our primary selection, secondary targets were identified in the bluer, $0.3 < W1 - W2 < 0.55$ colour region and tertiary targets in the $0.3 < W1 - W2 < 0.55$ and $1.8 < i - z < 2.2$ region of colour space. The bluer WISE cut was motivated by the presence of two previously discovered SDSS quasars of this colour which our original selection criteria of C15 miss. Whilst the region lies closer to the L dwarf locus it provided a test of the incompleteness of our more conservative $W1 - W2$ selection.

In total, we identified two candidates of highest priority within our primary selection region. These candidates were identified as highest priority due to their high signal-to-noise ratio (SNR) detections. A further seven primary candidates in areas of higher background noise and/or near CCD edges were also identified, along with ten secondary and five tertiary candidates in the VST ATLAS footprint, as observable from La Silla in our May 2015 NTT EFOSC2 observing run (see Section 4.2 below).

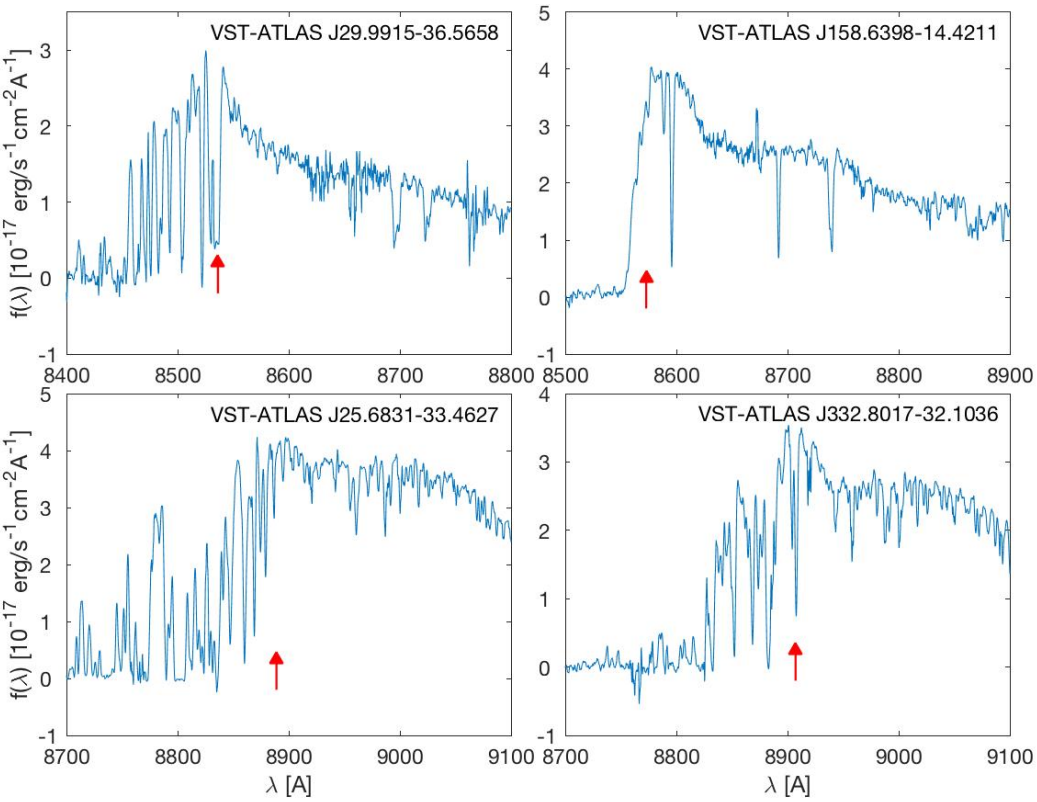

Figure 3. The VLT X-shooter spectra for our 4 ATLAS quasars now 'zoomed in' to emphasise the HI absorption structure around the Lyα emission line. The positions of the Lyα emission lines as estimated from the maxima of the line profiles are indicated by the red arrows.

4 FOLLOW-UP SPECTROSCOPY

4.1 Keck LRIS Spectroscopy

4.1.1 VST-ATLAS J158.6938-14.4211

On 2015 April 19 we observed one of our two highest priority candidates with the Low Resolution Imaging Spectrometer (LRIS Oke et al. 1995; Rockosi et al. 2010) on the Keck I telescope. The observers were X. Prochaska (P.I.), J. Hennawi and C. Leibler. The target was VST-ATLAS J158.6938-14.4211, which was observed for 600 s through a 1″ wide slit. We used the 400/8500 grating in the red arm giving ≈ 6.9Å resolution and a dispersion of 1.16Å/pixel and the 400/3400 grism in the blue arm giving ≈ 7Å resolution and a dispersion of 1.09Å/pixel. The LRIS spectrum of J158.6938-14.4211 was reduced with the LowRedux pipeline[3]. First, the pipeline processes the calibrations (bias, flat fields and sky flats) and computes the wavelength solution using arc lamps. Next, these calibrations are applied to the raw science frames, and a 1D spectrum is extracted from the 2D frames. The spectra are then flux calibrated using observations of a spectrophotometric standard star. The LRIS spectrum showed strong Lyα emission, cut off sharply towards blue wavelengths due to a strong Gunn-Peterson hydrogen absorption trough, confirming this as a quasar with an approximate redshift of $z = 6.05 \pm 0.03$ (but see Section 4.3 and Table 2). Also detected in emission are Lyβ, NV(1240 Å), OI(1304 Å) and SiIV(1398 Å). Other details of this quasar, including i, z, $W1$ and $W2$ magnitudes are given in Table 1.

4.2 ESO NTT/EFOSC2 Spectroscopy

4.2.1 VST-ATLAS J332.8017-32.1036

On 2015 May 29 we observed our second highest priority candidate with the European Southern Observatory's Faint Object Spectrograph and Camera 2 (EFOSC2, Buzzoni et al. 1984) on the 3.58m ESO New Technology Telescope (NTT). The observers were B. Chehade and T. Shanks and the target was VST-ATLAS J332.8017-32.1036. The target was observed for 600s through Grism No. 2 (100 lines/mm) and a 1″ wide slit giving a resolution of 49.6Å (FWHM). The pixels were binned

[3] http://www.ucolick.org/~xavier/LowRedux/index.html

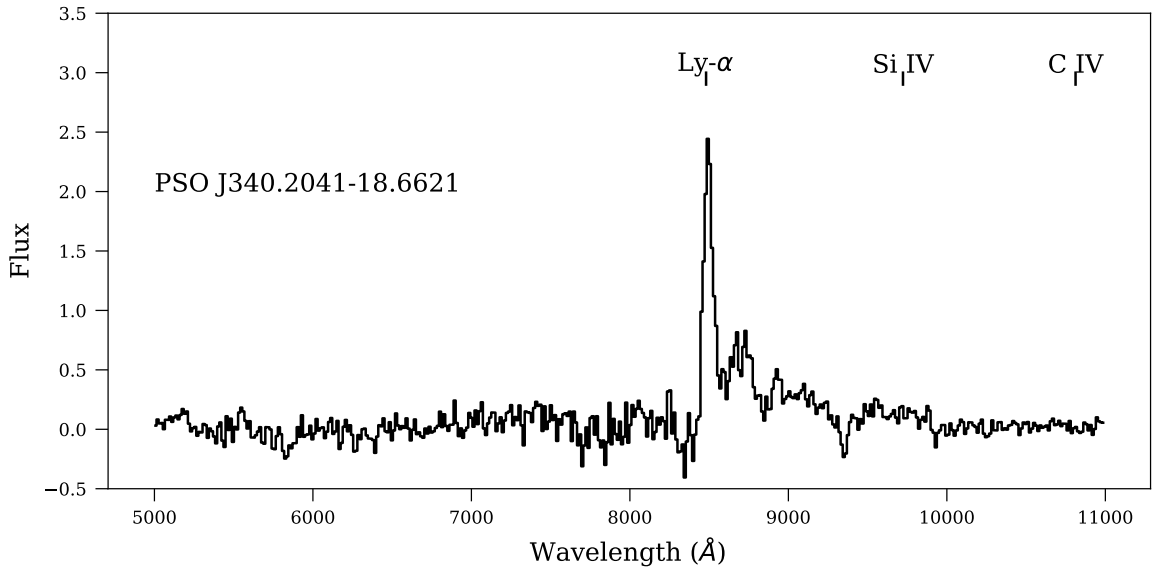

Figure 4. NTT/EFOSC2 spectrum for the re-discovered quasar PSO J340.2041-18.6621 of Bañados et al. (2014). The positions of $Ly\alpha$, $SiIV$ and CIV emission lines at $z = 5.98$ are shown.

2×2 in order to reduce readout time and noise. The resulting spatial scale was 0.25″/pixel and the dispersion was 13.2Å/pixel. All stages of the data reduction were performed using standard IRAF routines. The wavelength calibration was performed against Helium-Argon (HeAr) arc lamp spectra. The spectra cover the wavelength range of ≈ 5100−11000Å. Observations of the spectrophotometric standard star LTT3864 (Hamuy et al. 1992, 1994) were used for absolute flux calibration.

As with VST-ATLAS J158.6938-14.4211, strong Lyα emission was seen redwards of a Gunn-Peterson absorption trough, again confirming that this object was correctly identifed as a high redshift quasar with approximate redshift of $z = 6.37 \pm 0.03$ (but see Section 4.3 and Table 2). The NV (1240Å) emission line might also be detected at 9140Å. There is also a hint of Lyβ emission at 6520Å. Further discussion of these spectral features is postponed to Section 4.3, in which we report higher resolution X-shooter spectroscopy. Magnitudes for this quasar are also reported in Table 1.

4.2.2 PSO J340.2041-18.6621

A third high redshift quasar was observed with NTT EFOSC-2 on the night of 2015 June 01. Using the same VST ATLAS+WISE combined selection technique, we re-discovered the $z = 5.98$ quasar, PSO J340.2041-18.6621, independently found by Bañados et al. (2014) using the PanSTARRS survey. The spectrum confirmed the object as a quasar although we measured a slightly lower redshift of $z = 5.98 \pm 0.03$, based on the Lyα emission line, than that measured by Bañados et al. (2014) of $z = 6.03$. We include this quasar in Table 1 for completeness and its NTT spectrum is shown in Fig. 4.

4.3 VLT X-shooter Spectroscopy

To increase the wavelength coverage for the spectroscopically confirmed quasars from this work and C15 we observed the four VST ATLAS quasars with the medium resolution spectrograph X-shooter (Vernet et al. 2011) on the Cassegrain focus of the 8.2m VLT Kueyen (UT2) on the dates shown in Table 2. The X-shooter spectra are shown in Fig. 2.

The three arms of the X-shooter instrument are the UVB (3000 – 5595Å), the VIS (5595 – 10240Å) and the NIR (10240 – 24800Å). Given the redshift of our targets, we disregard the UVB arm data in our present analysis. The slit width for both the VIS and NIR arms was 0.″9 and slit length was 11″. Pixel scales are ∼ 0.15Å/pixel and ∼ 0.2Å/pixel for the VIS and NIR arms respectively. The resolution of the observations were $R \approx 7400$ in the VIS arm and $R \approx 5400$ in the NIR arm. We observed each of the 4 targets for 1hr each, ≈ 45 mins of which was on-sky exposure. The X-shooter spectra are shown in Fig. 2.

To reduce the X-shooter data, we built a tailor made workflow that incorporates both standard ESO recipes but also IRAF tasks to improve data quality. The ESO pipeline was used to perform the reduction steps up to the 2D rectified and merged spectrum. This includes bias subtraction, flat-fielding, modelling of the spectral orders, resampling and rectifying the spectra. We ensured that the default pipeline parameters were producing optimal results and adjusted them in a few cases, namely cosmic ray removal and sky background subtraction. To extract the QSO 1D spectra from the 2D spectra we used

the IRAF task apall. Finally, we applied a telluric correction to the NIR arm and merged the VIS and NIR arms to produce the spectra displayed in Fig. 2. Regions with transmission of less than ≈ 20% were masked from the spectra.

We show the positions of the Lyα, SiIV, CIV and MgII emission lines at the redshifts in Table 2; these are based on the X-shooter redshifts estimated from the position of Lyα indicated in Fig. 3. [4] Note the slight differences in these redshifts from those measured in the discovery spectra (see Table 1 and Table 1 of C15). The higher ionisation lines such as C IV are frequently seen to be blueshifted with respect to the lower ionisation lines (e.g Coatman et al. 2016) and this appears to be the case for these four quasars. However, it is not ruled out that there could be some uncertainty in our redshifts due to variation in the Lyα emission line profile. These issues are further discussed in Section 6 where redshifts are estimated from the CIV and MgII emission lines. The CIII] emission lines lie inside the range affected by atmospheric absorption in the X-shooter NIR data and so are unavailable to further test our redshifts. We note that quasar J332.8017-32.1036 may also show broad absorption features below the Si IV and C IV emission lines i.e. it may be a broad absorption line quasar (BALQ). We used these X-shooter spectra to measure $M_{1450\text{Å}}$ absolute magnitudes, as reported in Table 3. We also make a preliminary calculation of black hole masses in Section 6 but defer the detailed analysis and the fitting of Lyα emission and associated absorption line profiles (see Fig. 3) to future work (Diener et al., in prep.).

4.4 Other candidates and effect of relaxing the W1-W2 limit

Our original selection criteria as listed in Section 3 have produced the discoveries of four $z > 6$ quasars from the top of the ATLAS+WISE priority list. However, none of the other candidates which were also observed as part of our four night NTT run between 2015 May 29 and June 01, including our sample selected to be bluer in $W1 - W2$ and $i - z$, displayed spectral features consistent with high redshift quasars. These candidates had been marked as lower priority due to their lower signal to noise detections meaning a larger probability of these objects having scattered into our selection region from the stellar locus (see Fig. 1). We subsequently re-measured the i-band photometry for the i-band dropouts based in the z-band detections using the IMCORE routines supplied by CASU. The non-quasar targets were generally positively detected at below the 5σ limit of the ATLAS catalogue i.e. they were not i-dropouts.

5 CONSISTENCY WITH PREVIOUS QUASAR LUMINOSITY FUNCTION ESTIMATES

In this Section we will use our discovery of four (plus two re-discovered) $z > 6$ quasars from C15 and this work to check consistency with previous studies of the quasar luminosity function at bright absolute magnitudes. We estimate the completeness of our catalogues with respect to their depth and our ability to identify point-sources. Next, we test the completeness of our colour selections from Section 3. Finally, we check our completeness estimates against the Pan-STARRS survey of Bañados et al. (2016) before comparing our quasar space density to that expected from previous estimates of the quasar luminosity function.

5.1 Catalogue depths

To determine the completeness of VST ATLAS catalogues as a function of magnitude we need to compare the number of sources to the expected number of sources. We take advantage of the overlap between VST ATLAS and the PanSTARRS Medium Deep Survey (MDS, Chambers et al. 2016). The MD02 field of the MDS survey is covered by the VST ATLAS survey. The MD02 centre is RA 03:32:24, Dec -28:08:00 with a radius of ≈ 1.5deg. The approximate 5σ limits for this field in riz are 25.4, 25.8 and 25.3 mag (c.f. 22.7, 22.0 and 20.9 mag for VST ATLAS).

We wish to compare VST ATLAS exposures that are representative of the survey. To do this, we select a single VSTATLAS tile in each band with seeing similar to median seeing for the survey (0.″91, 0.″69, 0.″85 for the riz bands respectively).

Firstly, we assume that the MD02 field is complete and uniform to the depth that we test to (24th, 23rd and 22nd magnitude [AB] for the riz bands respectively). Given the dither pattern of the VST ATLAS survey different areas in the stack will either have two, one or no exposures. For each detection brighter than the faint limit in the MDS catalogue we compare to the VST ATLAS images, masking the MDS data according to the depth of VST coverage.

We compared `aper3` magnitudes from VST ATLAS to the Panstarrs PSF magnitudes and found offsets of $+0.06 \pm 0.03$, -0.19 ± 0.02 and $+0.08 \pm 0.03$ mag in the riz-bands. After correcting for these differences we can check VST ATLAS catalogue completeness.

In Fig. 5 we show the completeness of VST ATLAS catalogues compared to the Panstarrs MDS as a function of magnitude. We find that the catalogue is 99.6% complete to $z_{AB} = 20$, assuming that PanSTARRS is 100% complete..

[4] We prefer these Lyα redshifts rather than e.g. the MgII emission line redshifts given in Table 4 below on the grounds of the higher S/N of the Lyα line.

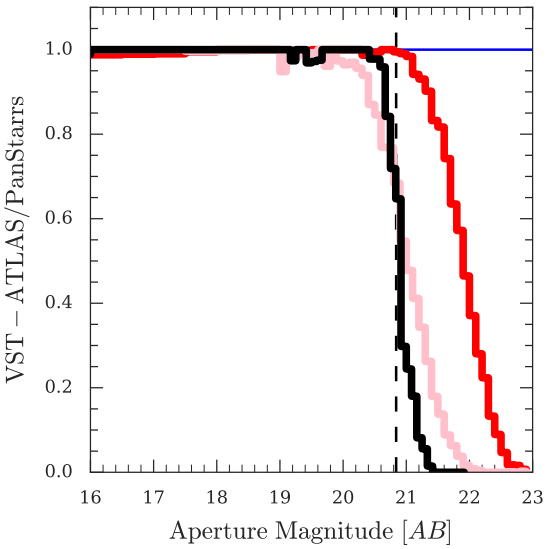

Figure 5. Completeness of the r, i and z-bands (red, pink and black respectively) as a function of magnitude. Fractions are derived by comparing catalogue detections in VST ATLAS with detections in the Panstarrs MD02 field. The vertical dashed line corresponds to the 5σ detection limit for the VST ATLAS z-band. The catalogue is 99.6% complete down to $z_{AB} = 20.0$ mag.

5.2 Point-source completeness

To remove contamination of our colour selection from local galaxies we select only point-sources as determined by their single band (z) morphological classification in the CASU catalogues. To test the completeness of the CASU morphological classification we modelled the difference between Petrosian and `aper1` (0.″5 radius) aperture magnitudes in the z-band for galaxies. We identified galaxies as all objects being 0.4mag brighter in Petrosian than in the `aper1` magnitude. We fit the distribution with a Gaussian model, allowing the centre, width and height to vary. We did this for all targets within four magnitude ranges; $18 < z < 18.5$, $18.5 < z < 19$, $19 < z < 19.5$ and $19.5 < z < 20$ mag. We excluded targets identified as noise (by their CASU `Classification`), targets in the singly exposed region and targets in regions with poorly fit sky background and de-blended photometry.

Fig. 6 shows the performance of the morphological separation of stars and galaxies in our faintest $19.5 < z_{AB} < 20.0$ mag range. Subtracting the modelled distribution of galaxies in the Petrosian-`aper1` plane to the distribution of all objects we may estimate the number of stars not identified as point-sources by CASU. We find the predicted extra number of stars in the above four bins (brightest to faintest) of 416, 837, 1277 and 704, implying 94%, 90%, 87% and 93% point-source completeness respectively. Increasing the aperture size to `aper2` (0.″7 radius) yields similar results for $z < 19$ but the separation in the Petrosian-`aper2` plane is less well defined so poorly fits the distribution of galaxies. Including these 'missed' stars to those identified by CASU we find an increase in the number of stars of 10%. Based on this analysis we estimate that our point-source completeness is 91%. This number agrees well with the estimate of Chehade et al. (2016) where stars were colour selected using multiple VST ATLAS and WISE bands.

5.3 Colour completeness

There are two methods used by other $z \sim 6$ quasar searches to calculate the incompleteness of their samples. The first is to clone low redshift quasar spectra and shift them to higher redshifts, (see Willott et al. 2005; Findlay et al. 2012). The second method, which we use in this work, is to create model quasar spectra based on empirical models of quasar SEDs (Fan et al. 1999; McGreer et al. 2013). Both methods assume that the low redshift UV properties of quasars, those redward of Lyα, do not evolve with redshift (Fan et al. 2004; Jiang et al. 2006).

To generate our model quasar spectra we use the publicly available `SIMQSO`[5] code developed by McGreer et al. (2013). In this code, each quasar is assigned a power law continuum with a break at 1100Å. The slopes are drawn from normal distributions based on the results of Telfer et al. (2002). Emission lines with Gaussian shape are added to this continuum and the emission line properties (wavelength, equivalent width and FWHM) are also drawn from normal distributions. The

[5] https://github.com/imcgreer/simqso

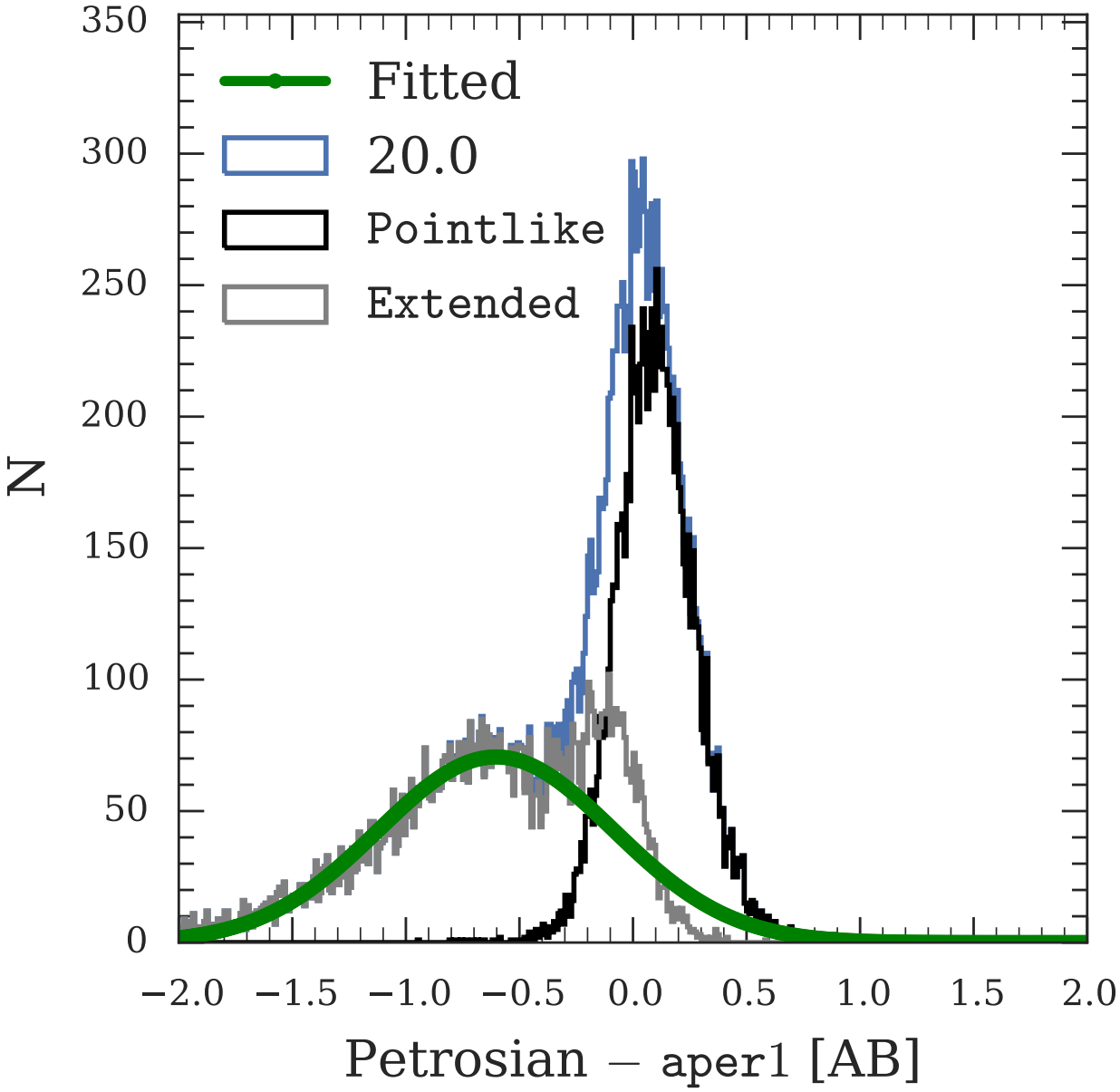

Figure 6. We show the distribution of Petrosian-`aper1` (0.″5 radius aperture) magnitudes in the z-band. The data consists of a single concatenation of seventeen tiles. The images were taken on night 2014-06-17 with median 0.″86 seeing (c.f. 0.″84 median for the survey). We plot the total histogram of objects (blue) between $19.5 < z_{AB} < 20.0$ mag i.e. the faintest 0.5 mag of our target candidates. The fitted galaxy distribution is shown as a solid green line. The black and grey histograms show the point-like and extended sources (as identified by CASU) respectively.

emission lines distributions are generated from composite BOSS spectra which have been stacked in different luminosity bins. The emission blueward of Lyα is based on the work by Worseck & Prochaska (2011). The model relies on the observed number densities of high column density systems (Songaila & Cowie 2010). A large number of sightlines are generated and the mean free paths are estimated by matching to the observations of Songaila & Cowie (2010). The column density distribution function is used to estimate the effective optical depth ($\tau_{\rm eff}$) which is checked for consistency with observations (Songaila 2004; Fan et al. 2006). Further details of the model may be found in McGreer et al. (2013). Note that we use the luminosity function parameters of Willott et al. (2010a). To accommodate WISE colour selection at higher redshifts we follow Yang et al. (2016),

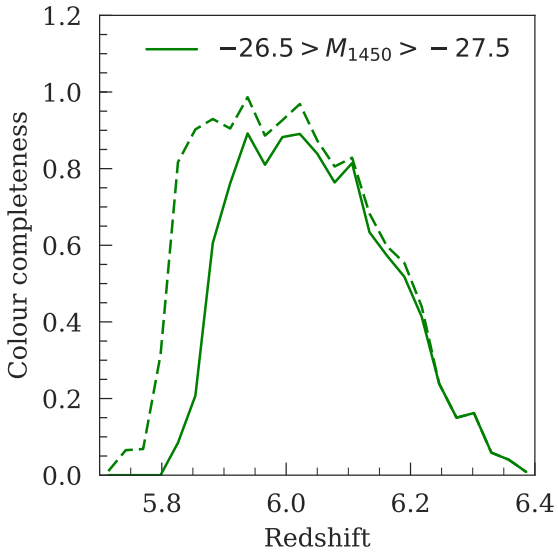

Figure 7. Colour completeness as a function of redshift. The solid line shows the completeness when we apply the most conservative selection from Section 3 and the dashed line shows the completeness using the relaxed selection criteria.

adding three new spectral breaks at 5700, 10850, and 22300Å and including their assumed spectral slopes and dispersions. Emission line parameters are derived from the composite quasar spectrum of Glikman et al. (2006).

We use `SIMQSO` to generate 140,000 model quasars evenly distributed between $5.7 < z < 6.4$ and $-26.5 \geq \mathrm{M}_{1450\text{Å}} \geq -27.5$. In Fig. 7 we show the resulting colour completeness using the photometric selections from Section 3. The completeness of the conservative selection rises sharply between redshifts $5.7 < z < 5.9$ due to the $i-z$ colour selection. When the colour selection is relaxed (shown by the dashed line) we see that the colour completeness is increased at lower redshifts. At higher redshifts ($z \gtrsim 6.05$) the completeness falls due to the faint limit of $z_{AB} = 20$ mag.

It should be noted that the 6 quasars in Table 3 show a redshift distribution apparently skewed to higher redshifts than implied by Fig. 7. Indeed, the `SIMQSO` quasar count model predicts that ~ 2/3 of detected quasars should lie in the $5.7 < z < 6.0$ range whereas only ~ 1/3 of those in Table 3 do. Indeed, the quasars selected by Bañados et al. (2016) are more consistent with this prediction. However, lacking any other explanation, we note that this larger than expected $z > 6$ fraction for ATLAS at least remains within the bounds of statistical error.

5.4 Completeness estimates checked via PanSTARRs

Bañados et al. (2016) have searched for $5.7 \leq z \leq 6.7$ quasars using the PanSTARRS1 (PS1) 3π survey. This survey covers the ATLAS sky footprint except for the areas below $Dec < -30$ deg in the SGC and NGC areas. Chambers et al. (2016) indicates that PS1 reaches ≈ 1.5 mag fainter than ATLAS in z, with a 5σ stellar limit of $z_{AB} = 22.3$ mag as opposed to $z_{AB} = 20.87$ mag for ATLAS. Bañados et al. (2016) quote a median limit of $z = 22.0$ mag for their PS1 survey. 5 extra quasars were detected in the ATLAS overlap area with $z_{AB} \leq 20.0$ mag; 4 of these had $z < 6$. One quasar was missed by ATLAS because it was classed as a galaxy (PSO J056.7168-16.4769), making an incompleteness of 1/7 or ≈ 14% of the 7 quasars that were detected by either survey in the ATLAS-PS1 overlap area. This is similar to our 10% star-galaxy incompleteness estimate. One quasar was missed on account of its $i-z$ colour being too blue (PSO J021.4213-25.8822) and two because either their $W1-W2$ colour was too blue (PSO J183.2991-12.7676) or there was no WISE counterpart within 3″ (CFHQS J1509-1749). This makes the colour incompleteness 3/7 or ≈ 43% compared to our incompleteness estimates of between 10-60% depending on redshift (see Fig. 7). We conclude that the extra quasars detected by Bañados et al. (2016) are not inconsistent with our star-galaxy separation and colour incompleteness estimates, although clearly there may still be further residual incompleteness associated with the PS1 survey.

5.5 Consistency with previous luminosity function studies

Following C15 we calculate $M_{1450\text{Å}}$ luminosities by scaling their SDSS composite template spectrum from Vanden Berk et al. (2001) and Songaila (2004) to the X-shooter spectra of each of our four ATLAS quasars in Fig. 2 using their observed Lyα redshift and z-band magnitude. The results are listed in Table 3, where we have also included the absolute magnitudes for

Quasar	Redshift	z (AB mag)	$M_{1450Å}$	Reference
ATLAS J025.6821-33.4627	6.31 ± 0.03	19.63 ± 0.06	-27.50 ± 0.06	Carnall et al. (2015)
ATLAS J029.9915-36.5658	6.02 ± 0.03	19.54 ± 0.08	-26.97 ± 0.08	Carnall et al. (2015)
VIKINGKiDS J0328-3253	5.86 ± 0.03	19.75 ± 0.12	-26.60 ± 0.04	Venemans et al. (2015a)
ATLAS J332.8017-32.1036	6.32 ± 0.03	19.75 ± 0.06	-26.79 ± 0.06	This paper
ATLAS J158.6938-14.4211	6.07 ± 0.03	19.44 ± 0.08	-27.23 ± 0.08	This paper
PSO J340.2041-18.6621	5.98 ± 0.03	19.67 ± 0.10	-26.42 ± 0.10	Bañados et al. (2014)

Table 3. Absolute magnitudes for the four quasars discovered and the two quasars rediscovered in VST ATLAS+WISE. The ATLAS quasar absolute magnitudes are estimated via the X-Shooter spectra in Fig. 2 and the other two from the above sources.

		CIV(1550Å)						MgII(2800Å)				
Quasar	z (LyA)	λ (Å)	z (CIV)	FWHM (kms^{-1})	v (kms^{-1})	$\lambda L_{1350Å}$ ($10^{44} ergs^{-1}$)	M_{BH} ($10^9 M_\odot$)	λ (Å)	z (MgII)	FWHM (kms^{-1})	$\lambda L_{3000Å}$ ($10^{44} ergs^{-1}$)	M_{BH} ($10^9 M_\odot$)
J029-36	6.024	10804	5.970	6425	-2306	198	1.4	19677	6.027	6510	440	6.4
J158-14	6.069	10864	6.009	7895	-2546	318	2.4	19806	6.073	2434	702	1.1
J025-33	6.305	11153	6.196	12255	-4476	224	2.2	20422	6.294	4109	448	2.6
J332-32	6.325	11214	6.235	12913	-3686	154	2.7	20516	6.327	3078	300	1.2

Table 4. Black hole masses estimated from the CIV and MgII broad emission line widths measured from the X-shooter NIR spectra. CIV and MgII wavelengths and FWHM widths are listed. $\lambda L_{1350Å}$ and $\lambda L_{3000Å}$ monochromatic continuum luminosities are based on z_{AB} and K_{AB} magnitudes. The K_{AB} magnitude for J025-33 is estimated from its z_{AB} and the mean $(z-K)_{AB} = 0.37$ colour of the other 3 quasars. CIV estimates of M_{BH} are from eqs. 4, 6 of Coatman et al. (2016) while MgII estimates follow eq. 1 of Vestergaard & Osmer (2009). Comparing the MgII and CIV values gives an approximate error for the average M_{BH} of ±37%.

our two re-discovered quasars quoted by Venemans et al. (2015a) and Bañados et al. (2014). We see that the 6 quasars occur in approximately one absolute magnitude bin centred on $M_{1450Å} \approx -27 \pm 0.5$.

We have estimated the quasar space density at $M_{1450Å} \approx -27$ based on our observations. We assume a search area of 3119 deg^2, representing 80% of the 3577deg^2 area searched i.e. assuming 20% area lost at CCD edges. From Fig. 7 and assuming the relaxed selection criteria of Section 3 we take the redshift range to be $5.7 < z < 6.4$. We take the redshift-dependent colour completeness to be that given in Fig. 7, the magnitude completeness at $z_{AB} < 20$ to be 100% and the star-galaxy separation completeness to be 90%, implying we need to multiply our 6 detected quasars by a factor of 1.9 to account for these incompletenesses. Thus our corrected quasar count is now 11.3 ± 4.6. We note that the total quasar count in the overlap area from Bañados et al. (2016) and ATLAS is 7 where ATLAS discovered 2, giving an ATLAS incompleteness factor of 3.5, compared to our modelled factor of 1.9. Applying this correction to the 6 ATLAS quasars gives a count of 21 ± 8.6 over 3119 deg^2. Although 1 out of 2 quasars available in Table 2 was missed by Bañados et al. (2016), we neglect this possible evidence for residual incompleteness in their sample on the grounds that the statistical error on the corrected count would be dominant. We conclude that the corrected number of quasars in our sample (11.3 ± 4.6) is in reasonable statistical agreement with those of Bañados et al. (2016) in a similar area (21 ± 8.6). As noted already, most of this difference is due to ATLAS missing $5.7 < z < 6$ quasars.

With a 3119 deg^2 survey area, our assumed, $\Omega_m = 0.3$, $\Omega_\Lambda = 0.7$, $h = 0.7$, cosmology indicates a volume of 17.4 Gpc^3 between $5.7 < z < 6.4$ and assuming a raw count of 6 ± 2.4 and an incompleteness corrected count of 11.3 ± 4.6 gives the quasar space density estimates shown in Fig. 8. Comparing these with the SDSS luminosity function of Jiang et al. (2016) and that of Willott et al. (2010a) at fainter magnitudes, we see there is good agreement between our observed number of quasars and the SDSS data which are bracketted by our raw and corrected space density estimates. Although our PS1 corrected space density would be $\approx 2\times$ higher than the corrected value shown, its $\approx 40\%$ error means there is still no significant disagreement with previous luminosity functions.

As an alternative view of how our quasar counts compare to previous work, we use the `SIMQSO` code of McGreer et al. (2013) with the luminosity function of Willott et al. (2010a) to predict the quasar count in the $15 < z_{AB} < 20$ mag and $5.7 < z < 6.4$ ranges. The predicted result is 8.1 ± 2.8 quasars in our 3119 deg^2 area. This compares to our raw, observed count of 6 ± 2.4 and our corrected count of 11.3 ± 4.6 quasars. We conclude that both these estimates are in good statistical agreement with the predicted value.

6 BLACK HOLE MASSES

Finally, we have made a preliminary estimate of the black hole masses powering these quasars. We therefore fitted Gaussian line profiles to the CIV and MgII lines in the NIR spectra from X-shooter using the IRAF splot routine. Table 4 shows the measured FWHM and central wavelengths of the emission lines. As can be seen from Fig. 2, the S/N for the CIV line is

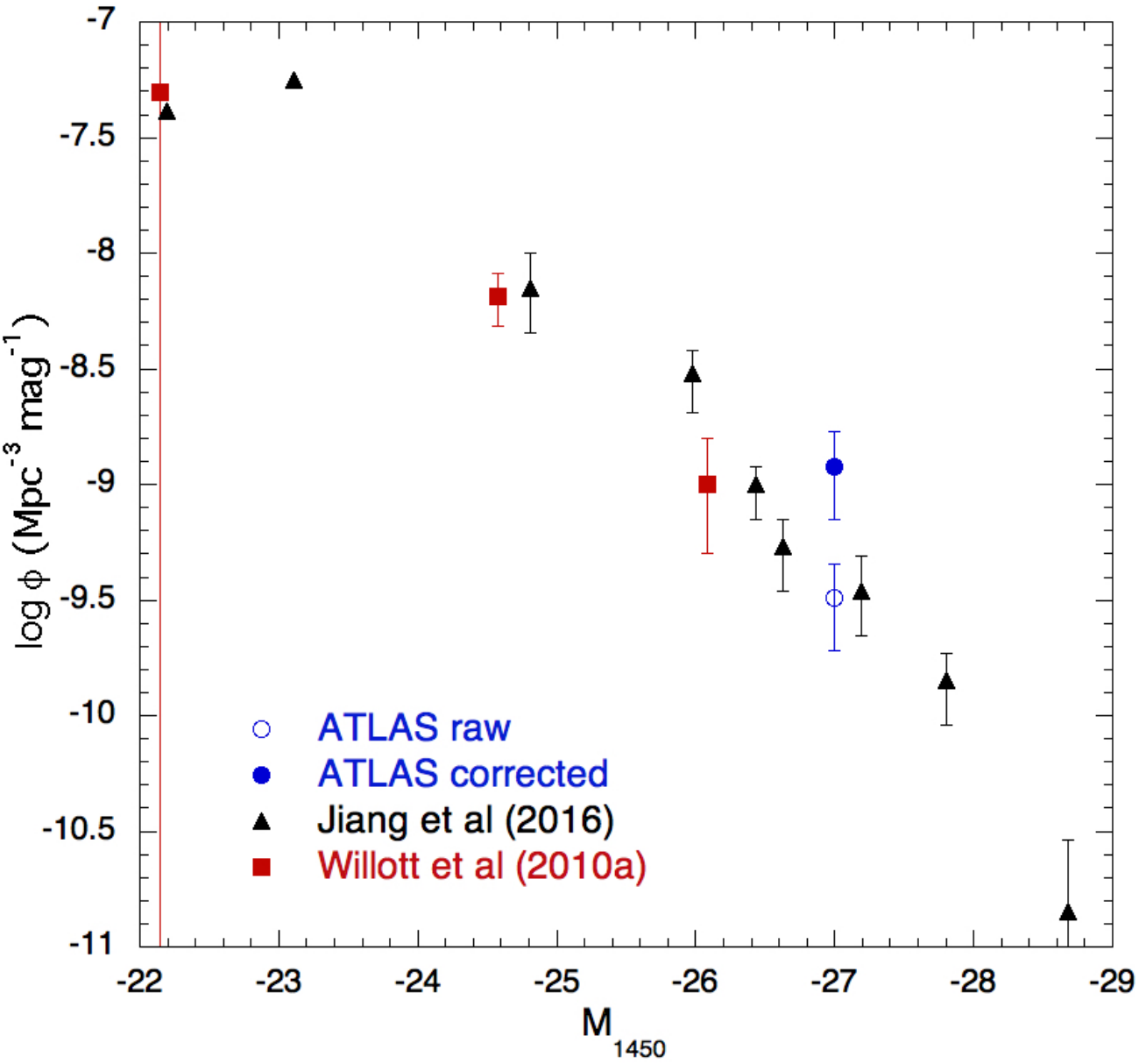

Figure 8. Approximate ATLAS quasar space densities at $M_{1450\text{Å}} = -27$ compared to the SDSS luminosity function of Jiang et al. (2016) and the fainter result of Willott et al. (2010a)corrected to our assumed cosmology. 'ATLAS raw' refers to six $5.7 < z < 6.4$ quasars detected in our 3119 deg^2 search and 'ATLAS corrected' refers to a corrected total of 11.3 quasars in the same volume.

generally higher than for MgII. The CIV lines can be seen to be blueshifted with respect to the redshifts based on the Lyα line as measured from the X-shooter spectra (see Fig. 3).

We estimated the monochromatic continuum luminosity, $\lambda L_{1350\text{Å}}$, for the CIV estimate from the quasar's z_{AB} band magnitudes and $\lambda L_{3000\text{Å}}$ for the MgII estimate from their K_{AB} magnitudes. We chose this route rather than using the X-shooter spectral fluxes from Fig. 2 partly on the grounds that the overall reliability of the spectrophotometry is uncertain and partly because the continuum at rest 3000Å lies at longer wavelengths than available from Fig. 2. If we assume that the spectrophotometry at 1350Å is accurate then our $\lambda L_{1350\text{Å}}$ estimates in Table 4 may be too large by a factor of ≈ 2 due to Lyα emission line contamination, implying that our resulting CIV M_{BH} estimates may be too large by $\approx 40 - 50\%$. There may be a similar systematic issue for the MgII M_{BH} estimates.

We then used eq. 4 of Coatman et al. (2016) to correct the FWHM of the CIV line for effects correlated with the CIV blueshift relative to lower ionisation lines.

$$FWHM(CIV,Corr.) = \frac{FWHM(CIV,Meas.)}{(0.41 \times CIV_{Blueshift}/1000kms^{-1} + 0.62)}$$

We then used their eq. 6 to estimate the values of M_{BH} given in Table 4.

$$M_{BH} = 10^{6.71} \times \frac{FWHM(CIV,Corr.)}{1000kms^{-1}} \times (\frac{\lambda L_{1350Å}}{10^{44}ergs^{-1}})^{0.53}$$

For the MgII based mass estimates we used eq 1 of Vestergaard & Osmer (2009) in the form:

$$M_{BH} = 10^{6.86}(FWHM(MgII))/1000)^2(\lambda L_{3000Å}/10^{44})^{0.5}.$$

We note that the errors on the MgII line widths will be substantial, especially for the lower redshift quasars whose lines are close to strong sky absorption features. The CIV FWHM are better measured but may have bigger systematic errors due to the large FWHM correction. With these caveats, the CIV and MgII masses appear to be in reasonable agreement, lying in the range $1-3\times10^9 M_\odot$ for CIV and $1-6\times10^9 M_\odot$ for MgII. Averaging both values gives $M_{BH} = 3.9, 1.8, 2.4, 2.0 \times 10^9 M_\odot$ respectively for J029-36, J158-14, J025-33 and J332-32 and averaging their standard errors gives a rough error estimate of ±37% on these mean values.

These compare to the $(1.24 \pm 0.19) \times 10^{10} M_\odot$ result for the $z = 6.3$ quasar of Wu et al. (2015), the brightest quasar ao far found at $z > 6$. This quasar has a monochromatic continuum luminosity of $\lambda L_{3000Å} = (3.15 \pm 0.47) \times 10^{47}$ erg s$^{\hat{a}\check{L}\check{S}1}$ some $\approx 5\times$ brighter than J158-14 which is our brightest quasar by this measure. J158-14 is $\approx 3\times$ less massive. Our four $z > 6$ quasars are generally similar in luminosity and mass to the $z = 7.05$ quasar ULAS J1120+0641 (Mortlock et al. 2011) and to the $z = 6.89$ quasar J0100+2802 (De Rosa et al. 2014), both with $M_{BH} \approx 2 \times 10^9 M_\odot$. The recently discovered $z = 7.54$ quasar (Bañados et al. 2018) has $M_{BH} \approx 7.8 \times 10^8 M_\odot$, significantly less massive than our four ATLAS quasars, likely due to lower continuum luminosity, it being ≈ 1 mag fainter in apparent K mag. and ≈ 0.5 mag. fainter given its luminosity distance and assuming zero K-correction.

These ATLAS quasars are therefore close to having some of the most massive black holes so far discovered and they lie at a redshift where they may cause significant difficulties due to the fast gravitational growth rates needed to explain their existence at such early times. A more detailed M_{BH} analysis, with improved error estimates and, e.g. where account is taken of the FeII emission surrounding MgII in measuring its line width, is postponed to a forthcoming paper.

7 CONCLUSIONS

Using similar combinations of VST ATLAS and WISE colours as C15 we have found a further two $z > 6$ quasars and rediscovered a third at a redshift $z \sim 6$. Adding these to the previous three found by C15 makes 6 quasars discovered in the searched ATLAS area of 3119 deg^2, corresponding to a volume of ~ 17.4 Gpc^3 between $5.7 < z < 6.4$. We confirmed the two new quasars using low dispersion spectroscopy at the ESO NTT and Keck telescopes and have presented X-shooter spectra for these and the 2 other quasars discovered in ATLAS. The initial criteria listed in Section 3 gave a 100% success rate for these 6 quasars which had the highest priority at the spectroscopic stage, indicating high selection efficiency. This possibly led to lower completeness rates and we have estimated the magnitude, star-galaxy separation and colour completenesses. When the joint effect of these incompletenesses are taken into account the corrected number of quasars rises to 11.3 ± 4.6. This corrected number is reasonably consistent with the discovery of a further 5 quasars detected in the overlap between the ATLAS and PS1 surveys by Bañados et al. (2016). We have compared our observed quasar space density at $M_{1450Å} \approx -27.0 \pm 0.5$ mag to the SDSS results of Jiang et al. (2016). Our raw and completeness corrected space densities bracket those of these authors and so can be considered in good agreement with the SDSS results. Finally, from preliminary virial analyses of the MgII and CIV broad emission lines we find black hole masses in the range, $M_{BH} \approx 1-6\times10^9 M_\odot$ for the four ATLAS quasars.

8 ACKNOWLEDGMENTS

Based on VST and VLT data products from observations made with ESO Telescopes at the La Silla Paranal Observatory under program ID's 177.A-3011(A,B,C,D,E.F,G,H,I,J), 294.A-5031(B), 095.A-0506(A) and 096.A-0418(A,B). Observations were also made at the Keck Telescope (Project U071LA, PI X Prochaska). This publication also makes use of data products from the Wide-field Infrared Survey Explorer, which is a joint project of the University of California, Los Angeles, and the Jet Propulsion Laboratory/California Institute of Technology, and NEOWISE, which is a project of the Jet Propulsion Laboratory/California Institute of Technology. WISE and NEOWISE are funded by the National Aeronautics and Space Administration.

We also thank the PanSTARRS1 collaboration for access to the Medium Deep Survey data in advance of publication. The

Pan-STARRS1 Surveys (PS1) have been made possible through contributions of the Institute for Astronomy, the University of Hawaii, the Pan-STARRS Project Office, the Max-Planck Society and its participating institutes, the Max Planck Institute for Astronomy, Heidelberg and the Max Planck Institute for Extraterrestrial Physics, Garching, The Johns Hopkins University, Durham University, the University of Edinburgh, Queen's University Belfast, the Harvard-Smithsonian Center for Astrophysics, the Las Cumbres Observatory Global Telescope Network Incorporated, the National Central University of Taiwan, the Space Telescope Science Institute, the National Aeronautics and Space Administration under Grant No. NNX08AR22G issued through the Planetary Science Division of the NASA Science Mission Directorate, the National Science Foundation under Grant No. AST-1238877, the University of Maryland, and Eotvos Lorand University (ELTE) and the Los Alamos National Laboratory.

We also acknowledge support from Science and Technology Facilities Council Consolidated Grant ST/P 000541/1.

Finally, we thank an anonymous referee for comments which have significantly improved the quality of this paper.

REFERENCES

Bañados E., Venemans B. P., Morganson E., Decarli R., Walter F., Chambers K. C., Rix H.-W., 2014, AJ, 148, 14
Bañados E., et al., 2016, ApJS, 227, 11
Bañados E., et al., 2018, Nature, 553, 473
Barnett R., Warren S. J., Becker G. D., Mortlock D. J., Hewett P. C., McMahon R. G., Simpson C., Venemans B. P., 2017, A&A, 601, A16
Becker R. H., et al., 2001, AJ, 122, 2850
Buzzoni B., et al., 1984, The Messenger, 38, 9
Carilli C. L., et al., 2010, ApJ, 714, 834
Carnall A. C., et al., 2015, MNRAS, 451, L16
Chambers K. C., et al., 2016, preprint, (arXiv:1612.05560)
Chehade B., 2016, PhD thesis, PhD thesis, Univ. of Durham, (2016)
Chehade B., et al., 2016, MNRAS, 459, 1179
Coatman L., Hewett P. C., Banerji M., Richards G. T., 2016, MNRAS, 461, 647
Crighton N. H. M., et al., 2015, MNRAS, 452, 217
De Rosa G., et al., 2014, ApJ, 790, 145
Fan X., et al., 1999, AJ, 118, 1
Fan X., Narayanan V. K., Lupton R. H., 2001, AJ, 122, 2833
Fan X., et al., 2004, AJ, 128, 515
Fan X., et al., 2006, AJ, 132, 117
Findlay J. R., Sutherland W. J., Venemans B. P., Reylé C., Robin A. C., Bonfield D. G., Bruce V. A., Jarvis M. J., 2012, MNRAS, 419, 3354
Fumagalli M., O'Meara J. M., Prochaska J. X., 2016, MNRAS, 455, 4100
Giallongo E., Grazian A., Fiore F., Fontana A., Pentericci L., Vanzella E., Dickinson M., 2015, A&A, 578, A83
Glikman E., Helfand D. J., White R. L., 2006, ApJ, 640, 579
González-Solares E. A., Walton N. A., Greimel R., 2008, MNRAS, 388, 89
Hamuy M., Walker A. R., Suntzeff N. B., Gigoux P., Heathcote S. R., Phillips M. M., 1992, PASP, 104, 533
Hamuy M., Suntzeff N. B., Heathcote S. R., Walker A. R., Gigoux P., Phillips M. M., 1994, PASP, 106, 566
Jiang L., et al., 2006, AJ, 131, 2788
Jiang L., et al., 2009, AJ, 138, 305
Jiang L., et al., 2016, ApJ, 833, 222
Kuijken K., et al., 2004, in Moorwood A. F. M., Iye M., eds, Proc. SPIEVol. 5492, Ground-based Instrumentation for Astronomy. pp 484–493, doi:10.1117/12.550892
Lehner N., O'Meara J. M., Howk J. C., Prochaska J. X., Fumagalli M., 2016, ApJ, 833, 283
Madau P., Haardt F., 2015, ApJ, 813, L8
Matsuoka Y., et al., 2016, ApJ, 828, 26
McGreer I. D., et al., 2013, ApJ, 768, 105
McLeod D. J., McLure R. J., Dunlop J. S., Robertson B. E., Ellis R. S., Targett T. A., 2015, MNRAS, 450, 3032
McLeod D. J., McLure R. J., Dunlop J. S., 2016, MNRAS, 459, 3812
Mortlock D. J., et al., 2011, Nature, 474, 616
Mortlock D. J., Patel M., Warren S. J., Hewett P. C., Venemans B. P., McMahon R. G., Simpson C., 2012, MNRAS, 419, 390
Oke J. B., et al., 1995, PASP, 107, 375
Parsa S., Dunlop J. S., McLure R. J., 2018, MNRAS, 474, 2904
Rafelski M., Neeleman M., Fumagalli M., Wolfe A. M., Prochaska J. X., 2014, ApJ, 782, L29
Reed S. L., et al., 2015, MNRAS, 454, 3952
Rockosi C., Stover R., Kibrick R., 2010, in Ground-based and Airborne Instrumentation for Astronomy III. p. 77350R, doi:10.1117/12.856818
Rosas-Guevara Y., Bower R. G., Schaye J., McAlpine S., Dalla Vecchia C., Frenk C. S., Schaller M., Theuns T., 2016, MNRAS, 462, 190
Shanks T., 2016, The Universe of Digital Sky Surveys, 42, 9
Shanks T., Fong R., Boyle B. J., 1983, Nature, 303, 156
Shanks T., et al., 2015, MNRAS, 451, 4238
Songaila A., 2004, AJ, 127, 2598

Songaila A., Cowie L. L., 2010, ApJ, 721, 1448
Telfer R. C., Zheng W., Kriss G. A., Davidsen A. F., 2002, ApJ, 565, 773
Vanden Berk D. E., et al., 2001, AJ, 122, 549
Venemans B. P., et al., 2013, ApJ, 779, 24
Venemans B. P., et al., 2015a, MNRAS, 453, 2259
Venemans B. P., et al., 2015b, ApJ, 801, L11
Vernet J., Dekker H., D'Odorico S., Kaper L., 2011, A&A, 536, A105
Vestergaard M., Osmer P. S., 2009, ApJ, 699, 800
Wang F., et al., 2015, ApJ, 807, L9
Wang F., et al., 2017, ApJ, 839, 27
Willott C. J., Delfosse X., Forveille T., Delorme P., Gwyn S. D. J., 2005, ApJ, 633, 630
Willott C. J., et al., 2010a, AJ, 139, 906
Willott C. J., et al., 2010b, AJ, 140, 546
Worseck G., Prochaska J. X., 2011, ApJ, 728, 23
Wotta C. B., Lehner N., Howk J. C., O'Meara J. M., Prochaska J. X., 2016, ApJ, 831, 95
Wright E. L., Eisenhardt P. R. M., Mainzer A. K., 2010, AJ, 140, 1868
Wu X.-B., et al., 2015, Nature, 518, 512
Yang J., et al., 2016, ApJ, 829, 33